Oblique angle co-deposition of nanocolumnar tungsten thin films with two W sources: Effect of pressure and target current

Valérie Potin, Houssem Boukhalfa, Nicolas Martin

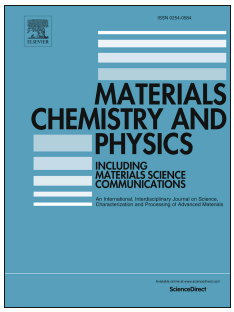

Oblique angle co-deposition of nanocolumnar tungsten thin films with two W sources: Effect of pressure and target current

Valérie Potin, Houssem Boukhalfa, Nicolas Martin

PII: S0254-0584(22)00170-5

DOI: https://doi.org/10.1016/j.matchemphys.2022.125864

Reference: MAC 125864

To appear in: *Materials Chemistry and Physics*

Received Date: 3 November 2021

Revised Date: 11 February 2022

Accepted Date: 13 February 2022

Please cite this article as: Valé. Potin, H. Boukhalfa, N. Martin, Oblique angle co-deposition of nanocolumnar tungsten thin films with two W sources: Effect of pressure and target current, *Materials Chemistry and Physics* (2022), doi: https://doi.org/10.1016/j.matchemphys.2022.125864.

Credit author Statement:

Valérie Potin: Writing – original draft, Writing – review & editing, Supervision, Funding acquisition

Houssem Boukhalfa: Data curation, Investigation

Nicolas Martin: Writing – review & editing, Supervision

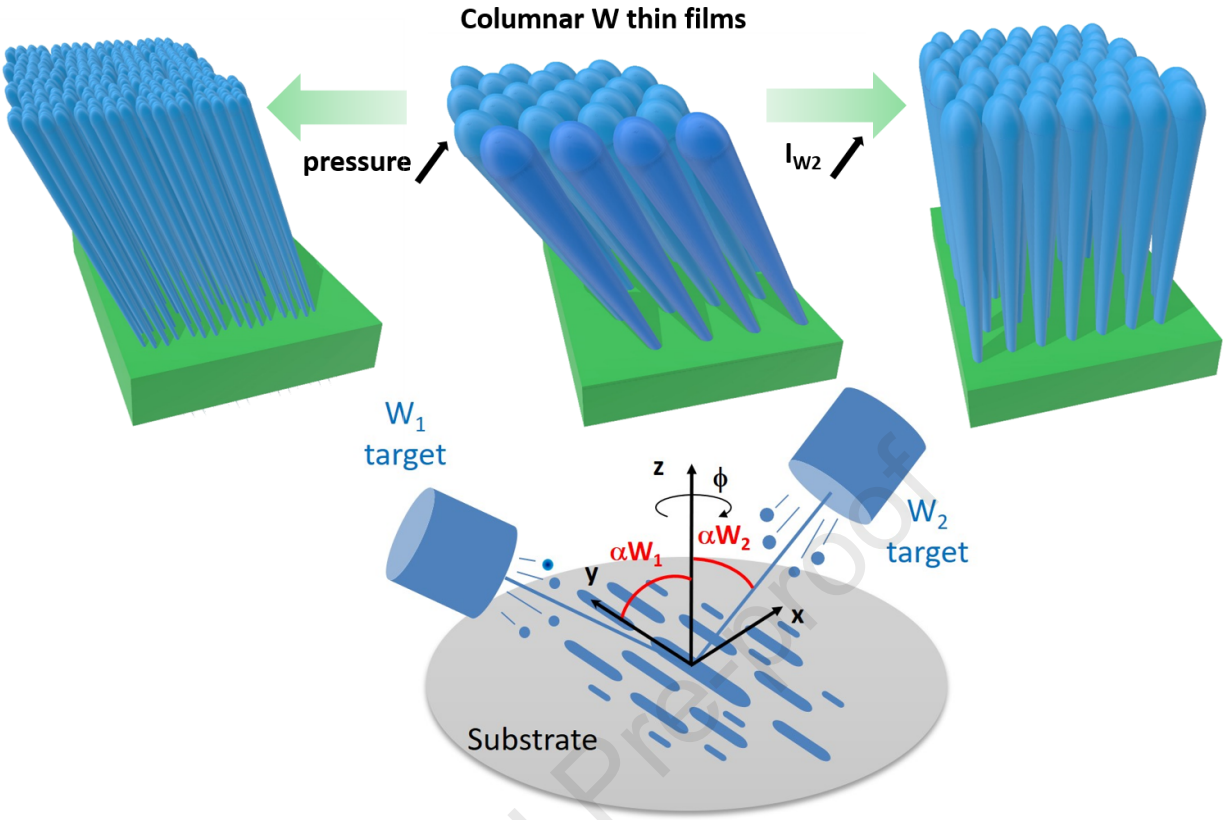

Oblique angle co-deposition of nanocolumnar tungsten thin films with two W sources: Effect of pressure and target current

Valérie Potin[1*], Houssem Boukhalfa[1] and Nicolas Martin[2]

[1]Laboratoire Interdisciplinaire Carnot de Bourgogne (ICB), UMR 6303 CNRS, Université Bourgogne Franche-Comté, 9, Avenue Alain Savary, BP 47 870, F-21078 Dijon Cedex, France

[2]Institut FEMTO-ST, UMR 6174 CNRS, Université Bourgogne Franche-Comté, 15B, Avenue des montboucons, 25030 Besançon Cedex, France

* Corresponding author: valerie.potin@u-bourgogne.fr

Graphical abstract

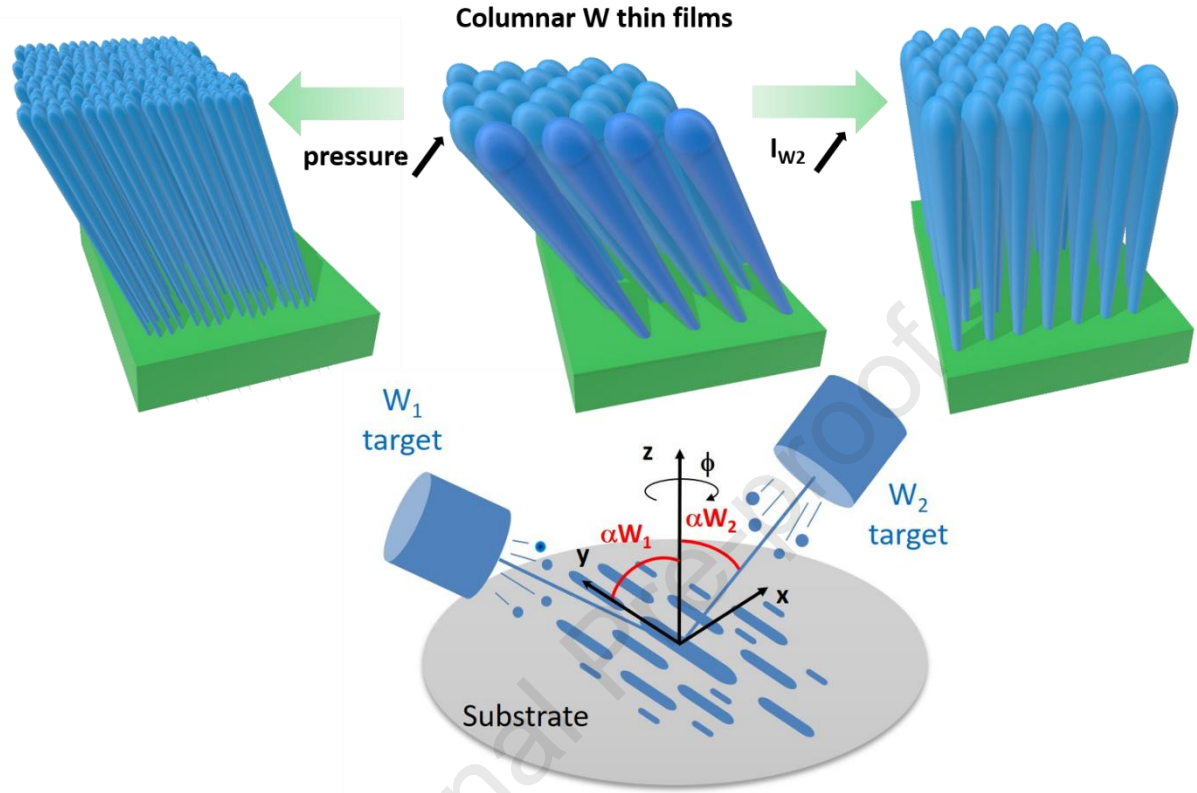

Abstract

Two series of tungsten thin films are sputtered on silicon and glass substrates by oblique angle co-deposition technique with an original configuration. Two opposite distinct tungsten targets are simultaneously used, both tilted with an oblique angle of 80°. The growth is performed at low (0.33 Pa) and high (1.5 Pa) argon sputtering pressure and the current intensity applied to the targets varies between 50 and 250 mA. The effect of these deposition parameters on the films microstructure and electrical properties is investigated by scanning and transmission electron microscopy, X-ray diffraction and pole figures, and van der Pauw method. Due to self-shadowing effect, all tungsten sputtered thin films are porous and columnar. At low pressure, the columnar tilt angle β can be tuned with the target current intensity until obtaining vertical columns. X-ray diffraction and pole figure analyses point out a A15 crystal structure (β-W) and a uniaxial fiber texture with a <100> growth direction. In contrast, tungsten thin films deposited at high pressure present a cauliflower structure and are poorly crystallized. Both deposition parameters also affect the films electrical resistivity and anisotropy. These behaviors are discussed and linked to the microstructure and crystallography.

Keywords: Tungsten, co-sputtering, GLAD, nanocolumns, microscopy.

1. Introduction

The modification of thin films properties due to oblique incidence of particles has been first reported by Knorr and Hoffman [1] and by Smith [2]. The oblique angle deposition (OAD) is mainly performed using physical vapor deposition (PVD) and is characterized by an oblique incidence of the incoming particle flux, as the source makes an angle α with the direction normal to the substrate [3]. As certain areas of the growing film are shadowed for direct impingement, a selective competition occurs between the shadowed and non-shadowed areas and the so-called "self-shadowing effect" results in anisotropic characteristics in thin films, eventually lessened by adatom surface diffusion [4-5]. Generally, OAD thin films are characterized by a higher porosity and tilted columnar structures in comparison to thin films elaborated with a normal incidence. This anisotropic microstructure generates anisotropic behavior in optical [6], magnetic [7] and electrical [8] properties. The porous character of the OAD thin films leads to an increased surface area that is a key parameter for many applications such as sensors, electrochemistry and catalysis [9-11]. The GLancing Angle Deposition (GLAD) is a technique derived from OAD that allows also to grow three-dimensional (3-D) nanostructures by altering the substrate motion and/or rotation [12-14]. Nanostructures including tilted or vertical columns, zigzags, S-shapes, C-shapes, spirals and helices are sculptured by modifying the polar (α) and azimuthal (ϕ) angles between the normal to the substrate and the incident deposition flux [10, 15]. The nanoarchitectured structures fabricated by GLAD technique have demonstrated enhanced capabilities in many applications including chemical and biological sensors, optical and electronic devices, magnetic storage as well as innovative coatings and applications [15-16].

To form multi-composition or multi-component structures, simultaneous or sequential oblique deposition of two materials from two different sources positioned at equal or different

angles has also been proposed [17]. Several systems were grown by OAD co-deposition technique with two different sources such as Fe-Cu [17], Co-M (M=Cr, Ag and Ta) [3] and Pt-M (M=Al, Si, Ti, Zr, Sn and Ce) [18] thin films. GLAD nanostructures were also obtained by co-deposition technique for Si-M (M=Cr, Pt, Ag, Cu and Ta) [19-20] as well as numerous metals, semiconductors and compounds [16]. By using two sources with oblique incidence, the morphology and/or elemental composition become also anisotropic. The 3-D growth is controlled by key parameters such as the angles of the incident fluxes, the deposition rates, the eventual substrate rotation/motion (and its speed) as well as usual deposition parameters [10, 15]. By modifying the deposition sequence (simultaneous or sequential) and the substrate rotation (stationary, continuous or intermittent), it is also possible to control the distribution of the components both laterally and vertically within the 3-D nanostructures [19, 21].

OAD and GLAD co-depositions are generally performed with two different materials obliquely deposited from two different targets. Only a few studies were performed on thin films prepared with two sources of a similar material. In 1981, Keitoku and Nishioka studied the grain structure and magnetic anisotropy of Fe films evaporated obliquely from two iron sources [17]. They reported that the iron films were formed by vertical columns, with an inclination of the columns with respect to the substrate surface normal almost equal to zero. This was in contrast with the columnar tilt angle equal to 45° measured for Fe films elaborated with a similar angle of incidence but with only one iron source [22]. In 1995, Robbie *et al.* [12] evaporated MgF_2 films by using two similar and opposite sources and obtained very porous thin films with isolated columns separated by large voids. In 2006, Kesapragada and Gall [23] deposited Cu nanorods on a patterned Si substrate using two opposite Cu sources. A two steps GLAD process was performed with continuous substrate rotation followed by deposition on stationary substrate. The first step

led to vertical columns and the second one to anisotropic broadened columns with an increase of the nanorod width in the direction parallel to the fluxes.

In this study, we report on the oblique angle deposition of tungsten thin films by magnetron sputtering using two opposite targets of tungsten. Former studies have been performed on tungsten (with one target) [8, 24], W-WO_3 [25], W-Cu [26-27] and W-Ag [28] deposited by magnetron sputtering in OAD configuration. Structure and electrical properties of such thin films are clearly dependent on the deposition parameters, mainly the sputtering pressure and the current intensity applied to the targets. Typically, if one the fluxes is dominant, it can largely influence the microstructure and the elemental composition of the thin films. Thus, by varying the current intensity applied to the targets, W-to-Cu and W-to-Ag atomic concentration ratio is tuned from 0.2 to 10 [26, 28]. In order to better understand the influence of these deposition parameters on the morphology and the electrical resistivity, OAD thin films have been deposited using two similar W targets. Several deposition parameters such as sputtering pressure, deposition temperature, oblique incidence angle have been reported to influence the growth and the final microstructure of the OAD and GLAD thin films [10]. So, for this study, many parameters such as α angles, deposition temperature, distances between the substrate and the targets are fixed during the deposition. Only two deposition parameters have been modified: the argon pressure and the intensity of the current applied to the targets. To investigate the influence of the sputtering pressure on the microstructure of the films, two argon sputtering pressures are chosen: 0.33 Pa and 1.5 Pa. Moreover, the current applied to one of the tungsten targets is set to 140 mA whereas the current to the second one is varied from 50 to 250 mA. The influence of these parameters on the morphology, crystallography and electrical resistivity of the tungsten thin films is studied and discussed.

2. Material and methods

Thin films are deposited by DC magnetron sputtering from two opposite tungsten metallic targets (both are 51 mm diameter and 99.9 at.% purity) on silicon and glass substrates (size of 25 × 12 mm^2) (Fig. 1).

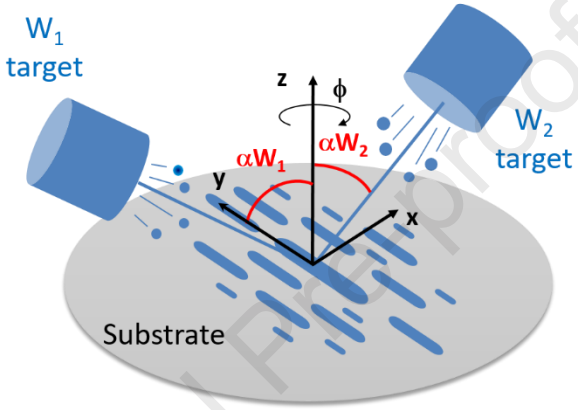

Fig. 1: Schematic representation of the OAD setup. Two tungsten targets W_1 and W_2 are tilted with fixed angles $\alpha W_1 = \alpha W_2 = 80°$. The target-to-substrate distances are fixed to 65 mm for W_1 and to 95 mm for W_2. The substrate can be fixed or rotated following the ϕ angle (not used in this study). W atoms are deposited on substrate defining a x-y plane whereas the z-axis is defined by the direction perpendicular to the substrate.

The deposition is performed at room temperature in a homemade 40 L vacuum chamber at a base pressure below 10^{-5} Pa. The distances between the center of the substrate and the center of W_1 and W_2 targets are equal to 65 mm and 95 mm, respectively. W_1 and W_2 targets are inclined according to the same incident angle equal to 80° defined by the normal to the substrate and the normal to the targets (αW_1 for W_1 target and αW_2 for W_2 target). The sputtering is performed simultaneously

at room temperature in a pure argon atmosphere. Two samples series are produced with two argon sputtering pressures of 0.33 and 1.5 Pa. The current of W_2 target is varied from 50 to 250 mA, IW_1 being kept unchanged at 140 mA. More details about the deposition facilities can be found in [26].

The films thickness measured by means of a Tencor Alpha Step IQ profilometer varies between 270 and 460 nm. The morphology of thin films deposited on silicon substrate is observed with a scanning electron microscope (SEM) Hitachi SU8230 from cross-section and surface views. The crystallographic structure of the W films is characterized by X-ray diffraction (XRD). Measurements are carried out using a Bruker D8 diffractometer with a copper line focus X-ray tube (Cu $\lambda K_{\alpha 1}$ = 0.154060 nm) with a θ/θ configuration. Scans are performed with a step of 0.0204° per 1 s and a 2θ angle ranging from 20 to 120°. The pole figures are performed using a Bruker D8 Discover GADDS diffractometer with a point focus cobalt X-ray tube. A 500 µm collimator is added to better focus the incident X-ray beam on the sample surface and the step size is 3° azimuthally (φ = 0°–358°). The transmission electron microscopy (TEM) analyses are performed using a JEOL 2100 FEG microscope with a 200 kV acceleration voltage. For TEM observations, scratched pieces of W thin films are dispersed on a lacey carbon film supported by a copper grid. TEM images are analyzed using the GATAN Digital Micrograph software and simulated with the Java Electron Microscopy Software (JEMS). The resistivity measurements are carried out at room temperature using the four probe van der Pauw method. The resistivity anisotropy is defined and measured [29] as the ratio between electrical resistivity following perpendicular and parallel directions to the sputtered particle fluxes [30].

3. Results and discussion

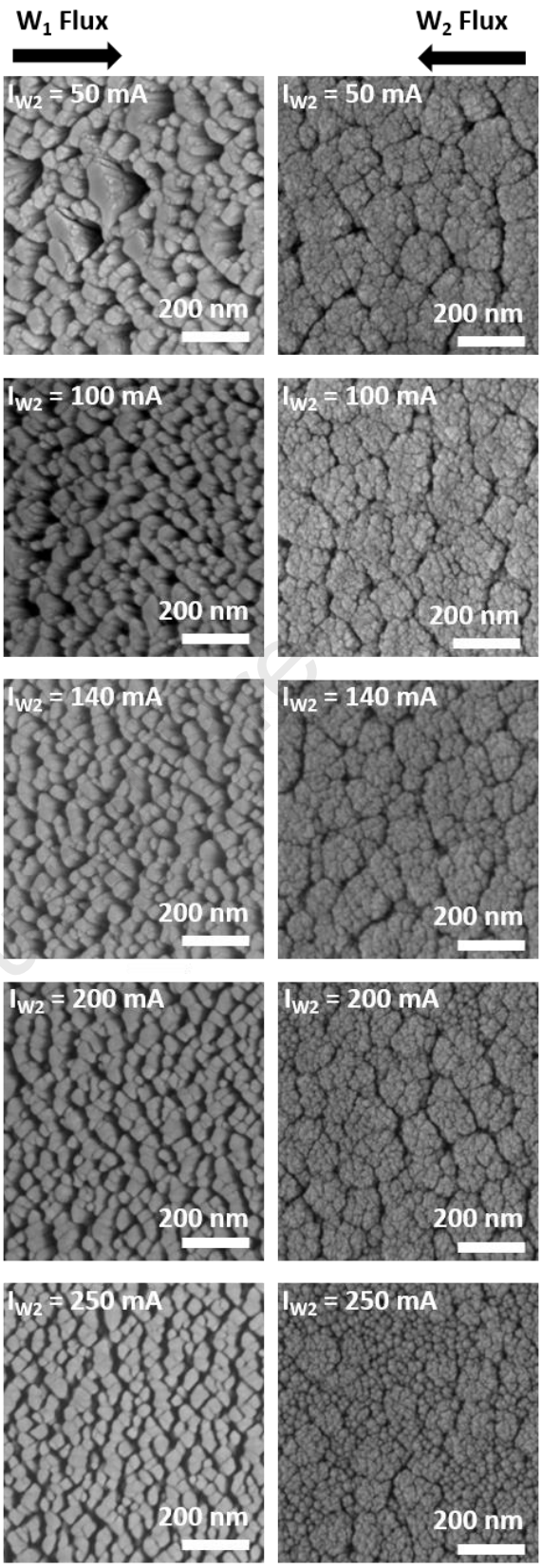

a) p = 0.33 Pa b) p = 1.5 Pa

Fig. 2: Top-view scanning electron microscopy observations of W thin films deposited at a) low pressure and b) high pressure with a constant target current (IW_1 = 140 mA) and various IW_2 target currents.

Top-view and cross-section scanning electron microscopy (SEM) images of the W thin films deposited at low (0.33 Pa) and high (1.5 Pa) argon sputtering pressures and with various W_2 target current intensities (IW_2 varying from 50 to 250 mA) are visible in Fig. 2 and 3. All SEM observations have been performed at the center of the samples, but are representative of the whole thin films' morphology, except at extremities. For all sputtering conditions, thin films appear as porous and columnar with separated and more or less inclined columns. It is well admitted that the morphology of OAD and GLAD thin films is mainly controlled by the self-shadowing effect [31], enhanced for high oblique incidence angle of the fluxes ($\alpha > 70°$). It can also be seen that the exhibited morphology strongly depends on the argon sputtering pressure. Indeed, surface SEM observations exhibit two kinds of morphology at both pressures (Fig. 2). At low pressure, the morphology appears to be asymmetric as some columns are connected forming elliptical structures perpendicular to the W particle fluxes. The bundled columns are also separated by elongated voids. This anisotropic microstructure has already been observed for tungsten thin films deposited by OAD with one source [8, 24] as well as for W-Cu and W-Ag thin films co-deposited by OAD [8, 28]. At high pressure, the morphology appears to be more isotropic with a cauliflower structure. Some voids separate the agglomerated columns and are also slightly perpendicular to the W particle fluxes. The agglomerated columns do not show the elliptical shape reported for thin films produced at low pressure, but rather a circular one. Therefore, the comparison of top-view SEM images indicates that W thin films are columnar, with agglomerated columns separated by voids. The growth is also more anisotropic for thin films produced at low pressure.

The phenomenon of asymmetric morphology and more specifically the coalescence of columns in a specific direction named "bundling" have been reported in many studies and are related to the one-dimensional nature of the shadowing effect [3, 10]. The bundling phenomenon consists in associating nanocolumns, laterally connected in a direction perpendicular to the particle flux. The formation of the bundled columns has been linked to a preferential trapping mechanism leading to a faster lateral growth of the nanocolumns, in the direction perpendicular to the particle fluxes until their coalescence [10]. In our study, as the two targets are opposite, shadowing effect still occurs in a one-dimensional way (incidence takes place in the x-z plane). As the growth keeps going on, nanocolumns are still merging in the direction perpendicular to the particle fluxes (y-direction) and the shadowing effect prevents the columns to be connected in the parallel direction (x-direction).

The difference of morphology at low and high pressures is linked to the more or less ballistic character of W sputtered atoms. At low pressure (0.33 Pa), ballistic sputtered particles are mainly produced and the particle fluxes are highly directional [10]. In contrast, a pressure increase corresponds to an increase of the density of argon atoms available for ionization. Therefore, at higher pressure, W sputtered particles undergo more scattering and the mean free path strongly decreases. The mean free path for sputtered W atoms in argon atmosphere is inversely proportional to the argon sputtering pressure following this equation (Eq. 1) [32]:

$$\lambda = \frac{k_B T}{\sqrt{2}\,\pi\,(r_{Ar}+r_W)^2\,p} \quad (1)$$

with k_B is the Boltzmann's constant (1.38×10^{-23} J.K^{-1}), T the temperature (300 K), p the pressure (Pa) and r_{Ar} = 97 pm and r_W = 130 pm the covalent radii of argon and tungsten, respectively. It is calculated equal to 55 mm for p = 0.33 Pa and equal to 12 mm for p = 1.5 Pa. Moreover, the target-

to-substrate distances being equal to 65 mm and 95 mm for W_1 and W_2 targets, respectively, the sputtered W particles are even more scattered at high pressure. Consequently, their kinetic energy decreases and the fluxes are also less directional. Thus, it can be considered that the W sputtered atoms evolve from a mostly ballistic behavior to a mostly thermalized one when the pressure changes from 0.33 to 1.5 Pa. The same behavior has been reported for W thin films grown by GLAD with one source ($\alpha = 85°$, constant rotation of the substrate) [33]. So, at higher pressure, thermalized particles experience numerous collisions and accordingly they are less directional than ballistic ones. Thus, the one-directional nature of the shadowing effect is altered and the anisotropic bundling phenomenon does not occur at high pressure. Finally, we note that both observed morphologies well correspond to the main features of γ and δ generic microstructures developed by theoretical model to describe the different growth regimes of gold thin films as a function of the oblique incidence angle α and the sputtering pressure [10]. δ-type microstructure described as vertical and coalescent columns with a high density of micropores is obtained for a high degree of thermalization whereas γ-type microstructure described as tilted and isolated columns is obtained for a low thermalization degree. In our deposition conditions, when the argon sputtering pressure increases from 0.33 to 1.5 Pa, the thermalization degree also increases from 0.5 to 3.2 and the microstructure evolves from a γ-type to a δ-type structures.

Cross-section SEM images reveal a columnar microstructure with columns inclined towards W_1 target (Fig. 3).

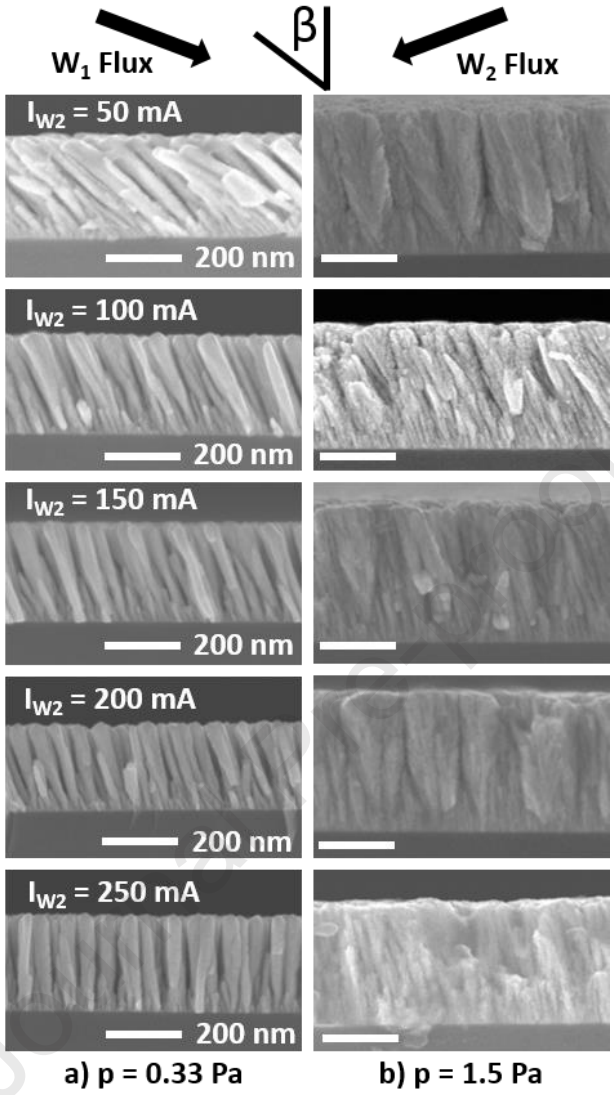

Fig. 3: Cross-section scanning electron microscopy observations of W thin films deposited at a) low pressure and b) high pressure with a constant target current (IW_1 = 140 mA) and various IW_2 target currents.

For all deposited films, thin columns are formed at the interface with the silicon substrate. Afterwards, during the growth, the thinnest columns disappear in favor of larger columns that widen. Consequently, the column's width increases with thickness. This column broadening is

linked to the extinction of small columns being shadowed by bigger ones. It has been reported that in the case of W thin films deposited by GLAD technique, columns width and length are related by a power law, with an exponent p = 0.34 [34].

Table 1: Deposition rate and columnar tilt angle (β angle) for W thin films prepared at low (LP) and high (HP) pressures with different IW_2 target currents.

	0.33 Pa (LP)		1.5 Pa (HP)	
IW_2 target current (mA)	Deposition rate ($nm.min^{-1}$)	β angle (°)	Deposition rate ($nm.min^{-1}$)	β angle (°)
50	8.2	39	17.7	11
100	11	22	13.2	18
140	10.4	16	19.7	10
200	10.5	15	22.3	3
250	12.5	3	25.5	8

The main evolution concerns the columnar tilt angle β defined as the angle between the normal to the substrate surface and the inclined columns direction (Fig. 3). Since W_1 target is closer to the substrate holder than W_2 target (65 mm and 95 mm, respectively), columns are oriented towards the W_1 particle flux, whatever the IW_2 current intensity applied to W_2 target. However, the increase of the IW_2 current leads to a decrease of the columnar tilt angle β. It is worth noticing that the influence of the W_2 particle flux becomes more visible as higher IW_2 currents are applied, especially at lower pressure. For these low pressure conditions, β presents a strong variation from 39° for IW_2 = 50 mA to 2° for IW_2 = 250 mA. In contrast, at high pressure, β is quasi constant with angles varying from 11° to 8° (Table 1). A comparison can be made with W thin films prepared with only one W target and with quite similar conditions (p = 0.35 Pa and p = 1.5 Pa, target-to-substrate distance = 65 mm, α = 80° and I_W = 140 mA) in the same homemade PVD chamber. At low and high pressures, W thin films exhibit a columnar tilt angle β equal to 39°

and 18°, respectively [24]. The value obtained for β at high pressure with one target is higher than all column angles obtained with two W targets, whatever the IW_2 current. At low pressure and with one target, β angle is similar to the maximum value obtained with two opposite W targets (for IW_2 = 50 mA). As the target-to-substrate distance is also shorter for W_1 than for W_2 target (65 mm versus 95 mm), one can even consider that the particle flux coming from W_2 target is negligible for IW_2 = 50 mA.

OAD thin films show a columnar morphology and are characterized by an inclination of the columns towards the particle flux direction. The columnar tilt angle β is systematically lower than the oblique incidence angle α. This value depends on many parameters such as the substrate temperature, the deposition rate and the partial pressure. Several models have been proposed to connect the columnar tilt angle β and the oblique incidence angle α [3, 14, 35-36]. Among the different empirical models, the tangent and the cosine rules have attracted much attention. The empirical "tangent rule" [37] gives better results for smaller α while the "cosine rule" suggested by Tait *et al.* [38] is proposed for larger α. For α = 80°, this is verified as the first equation predicts β = 71° and the second one β = 56°. However, these rules suppose that the relations between the angles are purely geometric and are not dependent on both materials and elaboration parameters [35]. This explains why some discrepancies are observed when one target is used and even more when the deposition takes place with two opposite targets [36].

Higher argon sputtering pressures lead to a strong decrease of W particle energy and directionality. Therefore, thermalization effect induces at high pressure a lesser influence of target currents on β angle [35]. In contrast, in the ballistic approach, the particles impinge on the film surface along straight and oblique trajectories. They remain at the landing location giving rise to tilted nanocolumns [10]. Due to the shadowing effect, deposited particles accumulate within

certain areas corresponding to the first location of growth. These grains lead to shadowing areas, preventing other particles to deposit within. This selective growth between shadowed and non-shadowed areas induces the formation of tilted columns towards the particle flux direction. In the case of two targets instead of one, an effective source direction must be considered [39]. But the growth mechanism with a strong influence of the self-shadowing effect still applies. As the two opposite W targets have a common plane (x-z plane), the self-shadowing effect occurs perpendicularly to this plane of incidence. This leads to a preferential aggregation of the grains perpendicular to the incident plane rather than parallel to it. Already deposited grains shadow adjacent regions from direct impingement. As the thickness increases, the self-shadowing effect is even more pronounced and a columnar structure with a specific orientation is obtained. The columnar grains aggregate along a row perpendicular to the plane of incidence. Since the two sources are symmetrically installed relative to the substrate axis, the particle fluxes would have the same contribution to the film growth (i.e., incoming fluxes and atom energies would be the same when impinging on the growing columns) leading to the deposition of vertical columns, as previously reported for Fe thin films by Keitoku *et al.* [17]. Otherwise, they will be inclined towards the most powered target in terms of flux and energy [16].

In our study, even if identical α angles are imposed, as the substrate-to-target distances are not equal for both sources (65 mm and 95 mm), the fluxes are not diametrically opposed. Thus, our configuration of the deposition system is not symmetric and the two incoming particle fluxes do not contribute equally to the columnar growth. Consequently, the angle β is not equal to zero for the same target current intensities and columns tilt towards the closest W_1 target. However, modifying the IW_2 current intensity allows to change the columnar tilt angle β. For IW_1 = 140 mA and IW_2 = 250 mA, quasi-vertical columns are obtained with $\beta = 2°$. The consequence of the more

important target-to-substrate distance for W_2 target compared to W_1 one is then compensated by the higher applied IW_2 current intensity, leading to balanced particle fluxes coming from the two opposite sides.

Fe, MgF_2 and Cu vertical columns were also previously obtained using two opposite sources of materials [7, 12, 19]. Instead of using two MgF_2 sources, Robbie *et al.* [12] proposed to use only one source and to rotate the substrate rapidly with 180° steps. However, zigzag structure was obtained instead of vertical columns. To control the columnar tilt angle independently of the film porosity, more complicated GLAD configurations have been proposed with specific parameters. For example, if α angle is kept constant whereas the substrate is rapidly rotated with a continuous or intermittent rotation, vertical columns are obtained [14, 40-41]. GLAD is a very useful technique to obtain 3-D nanostructures but it implies the control of polar (α) and azimuthal (ϕ) angles. OAD configuration with two opposite sources appears to be another method to easily obtain inclined or vertical columns, by simply playing on the target current intensity.

X-ray diffraction analyses point out differences for W thin films prepared at low and high argon sputtering pressure (p = 0.33 and 1.5 Pa). W thin films deposited at 0.33 Pa exhibit peaks largely more intense and clearly defined (Fig. 4-a). Thus, the decrease of the argon sputtering pressure is linked to a better crystallization. The most intense peak is detected at $2\theta = 35.55°$ and is assigned to the (200) planes ($2\theta = 35.52°$) of the body-centered cubic (bcc) β-W phase (ICDD-pdf # 65-6453). Its intensity strongly increases with the IW_2 current intensity. An asymmetric, broad and weak peak is recorded at a diffraction angle 2θ around 39.5°- 40.5° (Fig. 4-b). It is attributed to the sample deposited with IW_2 = 50 mA to a mixture of the (210) planes of the β-W phase and of the (110) planes of the α-W phase, respectively. For other IW_2 current intensities, the peak attributed to (110) planes of α-W phase is hardly distinguishable. For W thin films deposited

at high pressure, weaker diffracted signals with broader peaks are reported (Fig. 4-c). Both α and β phases of tungsten are reported with peaks recorded at 2θ = 35.44°, 39.88° and 40.25°, corresponding to β (200), β (210) and α (110) planes (2θ = 35.52°, 39.89° and 40.26°), respectively. If the intensities of the two last peaks are rather constant, the intensity of the first one also increases with IW_2 current intensity.

Previous studies have shown that tungsten is mainly formed in the thermodynamically stable body-centered-cubic (bcc) α-W phase, but can occur as a metastable cubic A-15 structure, also referred as β-W [42-45]. The unit cell of A15 structure is described as an ordered phase where the body centered lattice sites are occupied by O atoms whereas two lattice sites on each of the faces are occupied by W atoms. The lattices parameters are equal to a = 0.316 nm and a = 0.504 nm for α and β phases, respectively. The β-W phase is stabilized by the presence of oxygen acting as impurities, but without forming a tungsten oxide compound [42-43, 46-47]. Even if β-W is often described as an ordered A-15 unit cell with a W_3O stoichiometry, the tungsten thin films designated as β-W do not present an ordered structure and the oxygen concentration in the films is often below 15 at.% but does not reach the 25 at.%, corresponding to a W_3O stoichiometry [42-43, 47]. The stabilization of β-W has also been attributed to interstitial incorporation of argon or nitrogen impurities as well as to the stacking fault W_3W in the A15 structure [48-49]. The occurrence of α-W, β-W or a mixture of both is strongly sensitive to a variety of deposition parameters such as presence of underlayers and type of substrates, films thickness, pressure of inert or reactive gas, deposition temperature, substrate bias, deposition power as well as deposition rates [32, 44, 49].

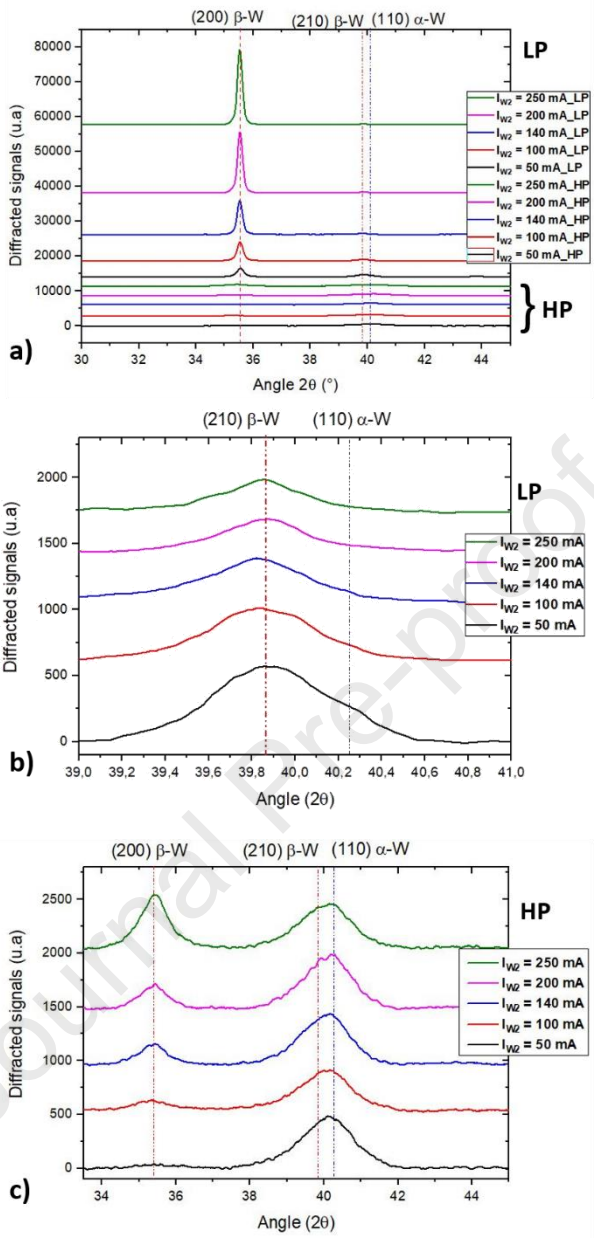

Fig. 4: X-ray diffraction patterns recorded in θ/θ configuration of W thin films prepared at low (LP) and high (HP) pressures with different IW_2 target currents: a) between 30° and 45°, b) zoom of the peak attributed to α-W (110) and β-W (210) superposition at around 40° (samples deposited at low pressure) and c) between 30° and 45° (increased y-scaling) for samples deposited at high pressure.

A better crystallinity has been reported for W thin films deposited at lower pressure by conventional sputtering [32] as well as for W thin films deposited by OAD or GLAD [24, 33]. It is due to the ballistic regime inducing lesser scattering and higher kinetic energy of W sputtered particles. This would also explain the higher intensity of (200) β-W peak with the increase of IW_2. A low sputtering pressure favors energetic W atoms and thus their diffusion on the growing film. In contrast, at high pressure, the lower energy, mobility and surface diffusion disrupt the crystallization process reducing the thin films' crystallinity. Khedir *et al.* [33] confirmed the preponderance of the metastable β-W phase at low pressure and of the stable α-W phase at high pressure. They proposed that oxygen atoms could more easily incorporate at interstitial positions at low pressure whereas Weerasekera *et al*. [46] have also linked the stability of the β-W phase to the amount of incorporated oxygen, more abundant at low deposition rate. In our case, the average deposition rate is equal to 10.5 $nm.min^{-1}$ at low pressure (p = 0.33 Pa) and to 19.7 $nm.min^{-1}$ at high pressure (p = 1.5 Pa) (Table 1). So, as the deposition rate increases at high pressure, the incorporation of residual oxygen would be more difficult and the β-W phase would be less stabilized at high pressure.

Using GLAD technique with continuous substrate rotation around the normal to the substrate, the β-W phase is reported to be favored compared to α-W one at low pressure [40]. Due to different adatom mobilities, the α-W and β-W phases are supposed to grow faster laterally and vertically, respectively. The shadowing effect favors the β-W phase that predominates over the α-W phase during OAD and GLAD growth. Using the two-step procedure proposed by Robbie *et al*. [14] with a fast rotation of 180° of the substrate followed by pauses for deposition, Krishnan *et al*. [41] also obtained vertical columns with β-W phase. With other GLAD parameters characterized by a "flipping rotation" mode, Chen *et al*. [45] reported the growth of vertical nanorods with the

α-W phase, the β-W phase being obtained under conditions similar to Karabacak *et al*. [40] (continuous substrate rotation). The occurrence of α-W phase was linked to a modification of the shadowing effect that is not enough efficient to promote the β-phase. Therefore, besides the aforementioned classical deposition parameters, OAD and GLAD parameters such as α angle, eventual motion and rotation of the substrate as well as in our case the two confocal W targets are additional deposition parameters that must be considered. This explains why it is not trivial to predict the occurrence of α and/or β phases as it is impacted by so many deposition parameters.

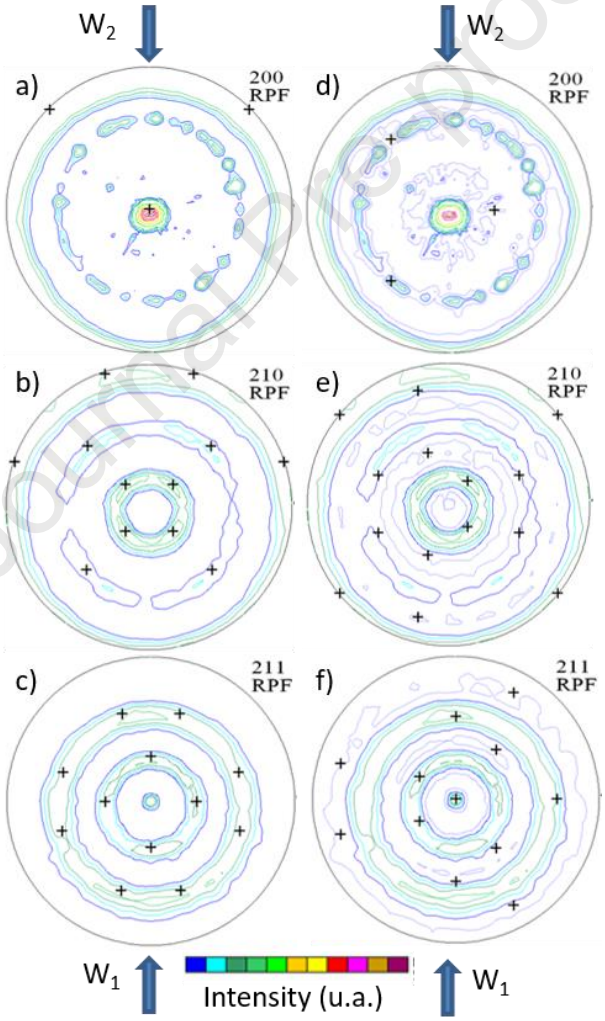

Fig. 5: a, d) {200}, b, e) {210} and c, f) {211} X-ray reconstructed pole figures (RPF) for the W thin films deposited at low pressure with IW_2 = 200 mA. The direction of the incident fluxes, indicated by arrows corresponds to the rolling direction. The crosses correspond to theoretical texture of {100} <011> (a-c) and {211} <0-11> (d-f).

X-ray pole figure measurements are performed on the sample deposited at low pressure with IW_2 = 200 mA to gain information about main texture component (Fig. 5). As the X-rays reach the silicon substrate, texture information is obtained from the whole deposited thin film. The reconstruction of pole figures (RPF) is performed (using Labotex software) for {200}, {210} and {211} planes of β-W, the first two ones corresponding to the two most intense XRD peaks (Fig. 3-a). The {200} reconstructed pole figure exhibits a very intense central spot, typical of {100} fiber pole figure, indicating that {200} are planes parallel to the surface. We note that a slight tilt could be applied with a shift towards {10 1 1} explained as the columns are not vertical for this sample but are inclined towards W_1 target with β = 14°. So, W columnar thin films are characterized by a strong {200} texture. Fig. 5-a also shows a quasi-continuous ring corresponding to {211} planes, pointing out the contribution of the fiber structure. In Fig. 5-b, the {210} RPF is characterized by the absence of a central spot and the presence of two quasi-continuous rings corresponding to {210} planes. Both features confirm the {200} texture and the fiber texture. A weak additional {211} fiber texture is present in Fig. 5-c as the {211} RPF exhibits a weak central spot and also in the {200} RPF (Fig. 5-d) with a weak secondary ring, suggesting an eventual secondary growth on the columns. Some fishbone-like shape secondary structures have previously been reported on the W-face of W-Cu thin films deposited by OAD [27]. The {200} texture combined to the fiber texture pointed out by RPF measurements indicates a random rotation of the

columns around preferential <100> growth direction. RPF method has not been applied to a sample deposited at high argon pressure as the XRD data indicate a poor crystallization. Moreover, the proximity of {210} β-W and {110} α-W would induce misinterpretations of the pole figures. We note that the surface energy of the different facets of α-W and β-W crystals has been calculated by density functional theory (DFT) energy calculations and reported in a database by Tran *et al*. [50]. For α-W, {110} planes exhibit the lowest surface energy with E = 3.23 $J.m^{-2}$ whereas {100} and {210} planes of β-W have the lowest and second-lowest surface energy with E = 3.29 $J.m^{-2}$ and E = 3.40 $J.m^{-2}$, respectively. Therefore, the exhibited {200} texture corresponds to the thermodynamically favored crystal planes of β-W.

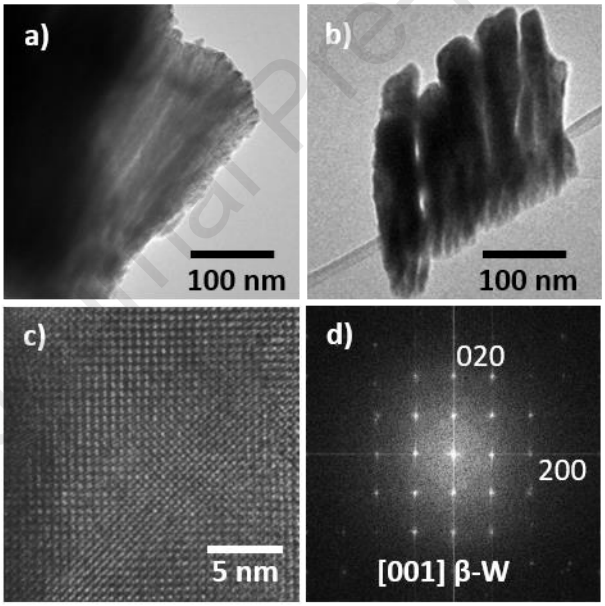

Fig. 6: TEM images of columnar W thin films deposited at a) high pressure and b) low pressure with IW_2 = 200 mA. c) HRTEM image of a crystallized area acquired for the sample grown at low pressure and d) its fast Fourier transform (FFT) pattern corresponding to [001] zone axis of β-W.

W thin films are also analyzed by high resolution transmission electron microscopy (HRTEM). Low-magnification TEM images are visible in Fig. 6-a and 6-b for the W thin films deposited at 1.5 Pa and 0.33 Pa (both with IW_2 = 200 mA). As the TEM samples have been prepared by scratching off, the silicon substrate is not visible. Figure 6-a confirms the columnar cauliflower structure already observed by SEM for samples deposited at high pressure. For sample deposited at low pressure, the columns are agglomerated and the coalescence effect is clearly visible as the width of the columns is smaller at their bottom part (Fig. 6-b). As the TEM samples have not been thinned down and as tungsten is a heavy element, only a few columns can be imaged for HRTEM. The W thin film deposited at high pressure displays a highly defective polycrystalline structure with crystallite size below 3 nm (not shown here), confirming the poor crystallization pointed out by XRD. In contrast, the sample deposited at low pressure displays some columns well orientated in zone axis (even if defective) and some HRTEM images have been recorded (Fig. 6-c). The analysis of the HRTEM images combined with calculated fast Fourier transform (FFT) patterns confirms that the columns are rather monocrystalline with a well-defined orientation (Fig. 6-d). They all correspond to a [001] zone axis with crystallographic {200} planes (d = 0.252 nm) of the β-W structure. These results agree with and confirm XRD and RPF ones. As the {200} planes are perpendicular to the growth direction of the columns, the growth direction corresponds to <100> direction and therefore, to the preferential growth direction of bcc crystals [50].

DC electrical resistivity and resistivity anisotropy are determined at room temperature for OAD W thin films deposited on glass substrate by the van der Pauw method. For samples deposited at low pressure, the resistivity gradually increases as a function of IW_2 current intensity from 1.15×10^{-5} to 4.85×10^{-5} Ω m (Fig. 7-a).

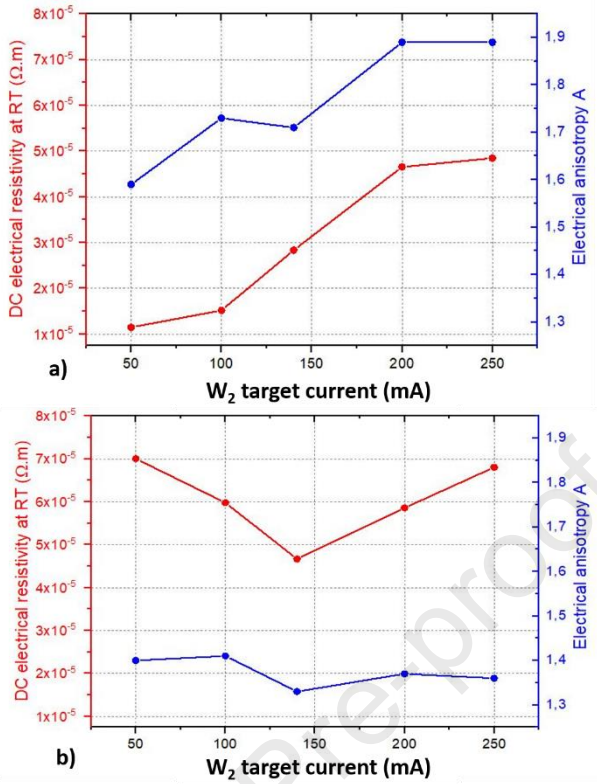

Fig. 7: DC electrical resistivity and resistivity anisotropy measured at room temperature as a function of the IW_2 target current for W thin films prepared by OAD with two W targets (IW_1 = 140 mA) at a) low (p = 0.33 Pa) pressure and b) high (p = 1.5 Pa) pressure.

These values are two or three orders of magnitude higher than the ones reported for bulk W (ρ_W = 5.44×10^{-8} Ω m) [51]. This higher resistivity is attributed to the enhancement of the electron scattering by surfaces and grain boundaries, more present in porous thin films. SEM observations have pointed out the presence of large voids between the tilted columns for W films deposited at low pressure. Moreover, it has been shown that the electrical resistivity depends on the crystallographic structure. Indeed, the electrical resistivity of α-W is one order of magnitude lower than β-W one [32, 40, 42]. This explains the gradual increase of the electrical resistivity for

samples grown at low pressure as it can be linked to the higher amount of β-W phase pointed out by XRD.

For samples deposited at high pressure, the resistivity also varies as a function of the IW_2 current intensity. It gradually decreases from 7.00×10^{-5} to 4.67×10^{-5} Ω m before rising to 6.80×10^{-5} Ω m (Fig. 7-b). Such resistivity values are higher than those previously measured for W films prepared at low pressure. At first, it can be assigned to the disordered structure recorded from XRD analyses (Fig. 4). Broad and low diffracted signals are systematically observed for W films deposited at high pressure, which corresponds to a low crystal size (a few nanometers) and thus, a reduced mean free path of electrons. The surprising minimum of resistivity observed for IW_2 = 140 mA can be explained neither from the evolution of the films' morphology (SEM pictures show similar top and cross-section features), nor by signification variations of the crystal structure (mixture of β-W and α-W phases poorly crystallized from XRD patterns). Although this minimum of resistivity at IW_2 = 140 mA remains an open question, one may suggest some correlations between the current IW_2, growing defects and proportion of β-W and α-W phases in the films. Assuming that a small grain size, the presence of stacking faults and the occurrence of the β-W phase favor a high film resistivity, the second W target is not only a source of matter but also supply energy from the incoming particle flux. For the lowest IW_2, W atoms diffusing on the columns side opposite to the W1 target migrate more easily to stable crystalline α-W growth sites, which reduces the films resistivity. A further increase of IW_2 and so, of the particle flux coming for the target W2 enhances the defect incorporation due to a growth competition between two particle fluxes. This competition favors the formation of the β-W phase (more intense β (200) diffracted signal at 2θ = 35.52° from XRD in Fig. 4) and thus, an increase of the resistivity is produced.

Using the Bierwagen method [29], the electrical resistivity has been measured in directions parallel (x-axis) and perpendicular (y-axis) to the particle fluxes. Then, the anisotropic resistivity is defined as the resistivity ratio following the parallel and perpendicular directions of the particle fluxes. At low pressure, the ratio is comprised between 1.59 and 1.89 whereas at high pressure, the ratio is nearly constant and close to 1.35. This anisotropic resistivity is linked to the elliptical shape already reported by SEM observations. In particular, the higher values obtained at low pressure correspond to an emphasized anisotropic morphology due to the bundling effect. The resistivity is favored in the direction parallel to the particle fluxes as the columns are separated by voids. Simultaneously, the conductivity is enhanced in the direction perpendicular to the particle fluxes as the columns are agglomerated along this direction because of the bundling effect. At high pressure, the constant electrical anisotropy is assigned to the less anisotropic and rather homogeneous cauliflower microstructure whatever IW_2 current intensity. Scattering of electrons is especially significant in this kind of microstructure since the bundled columns exhibit a small cross section as shown from SEM observations in figures 2 and 3. These nanocolumns are more or less connected to each other's and are separated by voids acting as barriers of potential for charge carriers.

4. Conclusion

In this study, a specific configuration is proposed to deposit tungsten thin films by co-sputtering on silicon and glass substrates using oblique angle deposition. The deposition is simultaneously performed from two distinct and opposite tungsten sources. Both targets are focused on the substrate with the same incident angle $\alpha = 80°$. Due to the shadowing effect, typical of OAD deposition, we observe that all samples are porous and columnar. The morphology,

crystallography and the electrical resistivity of the W thin films are tailored by the variation of argon sputtering pressure and current intensity applied to the second W target (IW_2). At low pressure, XRD analyses reveal the predominance of the metastable phase β-W and a <100> uniaxial fiber texture. Deposition at high argon pressure results in a cauliflower microstructure and a poor crystallization with a mixture of α-W and β-W phases. At low argon pressure (0.33 Pa), the columnar tilt angle β varies with IW_2 until obtaining vertical columns whereas samples deposited at high pressure (1.5 Pa) do not show any dependence. This work shows the meaningful effects of deposition conditions on the structure and morphology of tungsten films. Their modification as a function of the argon pressure is mainly linked to the occurrence of ballistic and diffusive regimes, inducing loss of energy and directionality of the particle fluxes.

CRediT authorship contribution statement

Valerie Potin: Writing - Review & editing. Houssem Boukhalfa: Data curation. Nicolas Martin: Writing - Review & editing.

Declaration of Competing Interest

The authors declare that they have no known competing financial interests or personal relationships that could have appeared to influence the work reported in this paper.

Acknowledgments

This work has been supported by the Region Bourgogne Franche-Comté and by EIPHI Graduate School (Contract ‘ANR-17-EURE-0002’). The authors are grateful to Loïc Chossemier, Nicolas

Geoffroy, Rémi Chassagnon and Cédric Thomas for helping in samples characterization and for fruitful discussions.

References

[1] T.G. Knorr and R.W. Hoffmann, Phys. Rev. 113 (1959) 1039–1046 "Dependence of Geometric Magnetic Anisotropy in Thin Iron Films"
https://doi.org/10.1103/PhysRev.113.1039

[2] D.O. Smith, J. Appl. Phys. 30 (1959) 264S-265S "Anisotropy in Permalloy Films"
https://doi.org/10.1063/1.2185921

[3] Herma van Kranenburg and Cock Lodder, Mater. Sci. Eng.: R: Rep. 11 (1994) 295–354 "Tailoring growth and local composition by oblique-incidence deposition: a review and new experimental data"
https://doi.org/10.1016/0927-796X(94)90021-3

[4] A. G. Dirks and H. J. Leamy, Thin Solid Films 47 (1977) 219–233 "Columnar Microstructure in Vapor-Deposited Thin Films"
https://doi.org/10.1016/0040-6090(77)90037-2

[5] Leon Abelmann and Cock Lodder, Thin Solid Films 305 (1997) 1–21 "Oblique evaporation and surface diffusion"
https://doi.org/10.1016/S0040-6090(97)00095-3

[6] D. Schmidt, A. C. Kjerstad, T. Hofmann, R. Skomski, E. Schubert and M. Schubert, J. Appl. Phys 105 (2009) 113508 (7pp) "Optical, structural, and magnetic properties of cobalt nanostructure thin films"
https://doi.org/10.1063/1.3138809

[7] Susumu Keitoku and Kazue Nishioka, Jpn. J. Appl. Phys. 20 (1981) 1249–1253 "Grain Structure and Magnetic Anisotropy of Fe Film Evaporated Obliquely from Two Sources"
https://doi.org/10.1143/JJAP.20.1249

[8] Raya El Beainou, Jean-Marc Cote, Vincent Tissot, Valérie Potin and Nicolas Martin, Surf. Coat. Technol. 421 (2021) 127412 (11pp) "Resistivity anisotropy of tilted columnar W and W–Cu thin films"
https://doi.org/10.1016/j.surfcoat.2021.127412

[9] V. Matolin, I. Matolinova, M. Vaclavu, I. Khalakhan, M. Vorokhta, R. Fiala, I. Pis, Z. Sofer, J. Poltierova-Vejpravova, T. Mori, V. Potin, H. Yoshikawa, S. Ueda and K. Kobayashi, Langmuir 26 (2010) 12824–12831 "Platinum-doped CeO2 thin film catalysts prepared by magnetron sputtering"
https://doi.org/10.1021/la100399t

[10] Angel Barranco, Ana Borras, Agustin R. Gonzalez-Elipe, Alberto Palmero, Progress in Materials Science 76 (2016) 59–153 “Perspectives on oblique angle deposition of thin films: From fundamentals to devices”
http://dx.doi.org/10.1016/j.pmatsci.2015.06.003

[11] Mykhailo Chundak, Ivan Khalakhan, Peter Kúš, Tomáš Duchoň, Valérie Potin, Arnaud Cacucci, Nataliya Tsud, Vladimír Matolín and Kateřina Veltruská, Mater. Chem. Phys. 232 (2019) 485–492 “Tailoring of highly porous SnO_2 and SnO_2-Pd thin films”
https://doi.org/10.1016/j.matchemphys.2018.11.022

[12] K. Robbie, L. J. Friedrich, S. K. Dew, T. Smy and M. J. Brett, J. Vac. Sci. Technol. A 13 (1995) 1032–1035 **“**Fabrication of thin films with highly porous microstructures”
http://dx.doi.org/10.1116/1.579579

[13] K. Robbie and M. J. Brett, J. Vac. Sci. Technol. A 15 (1197) 1460–1465 “Sculptured thin films and glancing angle deposition: Growth mechanics and applications”
https://doi.org/10.1116/1.580562

[14] K. Robbie, J. Sit, M. Brett, J. Vac. Sci. Technol. B 16 (1998) 1115–1122 “Advanced techniques for glancing angle deposition”
https://doi.org/10.1116/1.590019

[15] M. M. Hawkeye, M. T. Taschuk and M. J. Brett, Glancing Angle Deposition of Thin Films: Engineering the Nanoscale, John Wiley & Sons, Ltd, Chichester, UK, 2014

[16] Yuping He and Yiping Zhao, Nanoscale 3 (2011) 2361–2375 “Advanced multi-component nanostructures designed by dynamic shadowing growth”
https://doi.org/10.1039/c1nr10103j

[17] Susumu Keitoku Tatsuo Kamimori and Mitita Goto, Jpn. J. Appl. Phys. 25 (1986) 1668–1671 “Inhomogeneous Concentration Distribution in Obliquely Evaporated Fe-Cu Films”
https://doi.org/10.1143/JJAP.25.1668

[18] Yoshihide Watanabe, Shi-aki Hyodo, Tomoyoshi Motohiro, Tatsumi Hioki, Masahiro Sugiura and Shoji Noda, Thin Solid Films 256 (1995) 68–72 “Catalytic properties of thin films by simultaneous oblique sputter deposition of two materials from different directions”
https://doi.org/10.1016/0040-6090(94)06279-X

[19] S.V. Kesapragada, D. Gall, Thin Solid Films 494 (2006) 234–239 “Two-component nanopillar arrays grown by Glancing Angle Deposition”
https://doi.org/10.1016/j.tsf.2005.08.128

[20] Yuping He, Jinsong Wu, and Yiping Zhao, Nano Lett. 7 (2007) 1369–1375 "Designing Catalytic Nanomotors by Dynamic Shadowing Growth"
https://doi.org/10.1021/nl070461j

[21] C.M. Zhou, H.F. Li, D. Gall, Thin Solid Films 517 (2008) 1214–1218 "Multi-component nanostructure design by atomic shadowing"
https://doi.org/10.1016/j.tsf.2008.05.049

[22] Kazuhiro Hara, Takashi Hashimoto and Eiji Tatsumoto, J. Phys. Soc. Jpn. 28 (1970) 254 (1pp) "Origin of Anomalous Magnetic Anisotropy of Iron Films Evaporated at Oblique Incidence"
https://doi.org/10.1143/JPSJ.28.254

[23] S. V. Kesapragada and D. Gall, Appl. Phys. Lett. 89 (2006) 203121 (3pp), "Anisotropic broadening of Cu nanorods during glancing angle deposition"
https://doi.org/10.1063/1.2388861

[24] Asma Chargui, Raya El Beainou, Alexis Mosset, Sébastien Euphrasie, Valérie Potin, Pascal Vairac and Nicolas Martin, Nanomaterials 10 (2020) 81 (18pp) "Influence of Thickness and Sputtering Pressure on Electrical Resistivity and Elastic Wave Propagation in Oriented Columnar Tungsten Thin Films"
https://doi.org/10.3390/nano10010081

[25] Nicolas Martin, Arnaud Cacucci, Valérie Potin, Luc Imhoff and Tomas Nyberg, Mat. Lett. 172 (2016) 128–131 "Architectured columns with a metal-dielectric periodic nanostructure"
http://dx.doi.org/10.1016/j.matlet.2016.02.161

[26] Raya El Beainou, Nicolas Martin, Valérie Potin, Paulo Pedrosa, Mohammad Arab Pour Yazdi and Alain Billard, Surf. Coat. Technol. 313 (2017) 1–7 "Correlation between structure and electrical resistivity of W-Cu thin films prepared by GLAD co-sputtering"
http://dx.doi.org/10.1016/j.surfcoat.2017.01.039

[27] Raya El Beainou, Jean-Marc Cote, Valérie Potin and Nicolas Martin, Mater. Today Commun. 27 (2021) 102331 (4pp) "Contrasted morphologies in nanostructured Janus W-Cu columns"
https://doi.org/10.1016/j.mtcomm.2021.102331

[28] Houssem Boukhalfa, Valérie Potin and Nicolas Martin, J. Phys. D: Appl. Phys. 54 (2021) 255304 (9pp) "Microstructural analysis and electrical behaviours of co-sputtered W–Ag thin films with a tilted columnar architecture"
https://doi.org/10.1088/1361-6463/abf312

[29] O. Bierwagen, R. Pomraenke, S. Eilers, and W. T. Masselink, Phys. Rev. B 70 (2004) 165307 (6pp) "Mobility and carrier density in materials with anisotropic conductivity revealed by van der Pauw measurements"

https://doi.org/10.1103/PhysRevB.70.165307

[30] Kasper A. Borup, Karl F. F. Fischer, David R. Brown, G. Jeffrey Snyder and Bo B. Iversen, Phys. Rev. B 92 (2015) 045210 (10pp) "Measuring anisotropic resistivity of single crystals using the van der Pauw technique"
https://doi.org/10.1103/PhysRevB.92.045210

[31] D.O. Smith, M.S. Cohen and G.P. Weiss, J. Appl. Phys. 31 (1960) 1755–1762 "Oblique-Incidence Anisotropy in Evaporated Permalloy Films"
https://doi.org/10.1063/1.1735441

[32] F.T.N. Vüllers and R. Spolenak, Thin Solid Films 577 (2015) 26–34 "Alpha- vs. beta-W nanocrystalline thin films: A comprehensive study of sputter parameters and resulting materials' properties"
http://dx.doi.org/10.1016/j.tsf.2015.01.030

[33] Khedir R. Khedir, Ganesh K. Kannarpady, Hidetaka Ishihara, Justin Woo, Charles Ryerson and Alexandru S. Biris, Phys. Lett. A 374 (2010) 4430–4437 "Morphology control of tungsten nanorods grown by glancing angle RF magnetron sputtering under variable argon pressure and flow rate"
https://doi.org/10.1016/j.physleta.2010.08.066

[34] T. Karabacak, J. P. Singh, Y.-P. Zhao, G.-C. Wang, and T.-M. Lu, Phys. Rev. B 68 (2003) 125408 (5pp) **"**Scaling during shadowing growth of isolated nanocolumns"
https://doi.org/10.1103/PhysRevB.68.125408

[35] J. M. García-Martín, R. Alvarez, P. Romero-Gómez, A. Cebollada, and A. Palmero, Appl. Phys. Lett. 97 (2010) 173103 (3pp) "Tilt angle control of nanocolumns grown by glancing angle sputtering at variable argon pressures"
https://doi.org/10.1063/1.3506502

[36] Yiping Zhao, Yuping He and Cameron Brown, Appl. Phys. Lett. 100 (2012) 033106 (3pp) "Composition dependent nanocolumn tilting angle during the oblique angle co-deposition"
https://doi.org/10.1063/1.3676665

[37] J. M. Nieuwenhuizen and H. B. Haanstra, Philips Tech. Rev. 27 (1966) 87–91 "Microfractography of thin films"

[38] R. N. Tait, T. Smy and M. J. Brett, Thin Solid Films, 226 (1993) 196–201 "Modelling and characterization of columnar growth in evaporated films"
https://doi.org/10.1016/0040-6090(93)90378-3

[39] H. J. Leamy and A. G. Dirks, J. Appl. Phys. 49 (1978) 3430–3438 "Microstructure and magnetism in amorphous rare-earth–transition-metal thin films. I. Microstructure"

http://dx.doi.org/10.1063/1.325249

[40] Tansel Karabacak, Anupama Mallikarjunan, Jitendra P. Singh, Dexian Ye, Gwo-Ching Wang and Toh-Ming Lu, Appl. Phys. Lett. 83 (2003) 3096–3098 "β-phase tungsten nanorod formation by oblique-angle sputter deposition"
https://doi.org/10.1063/1.1618944

[41] R Krishnan, T Parker, S Lee and T-M Lu, Nanotechnology 20 (2009) 465609 (6pp) "The formation of vertically aligned biaxial tungsten nanorods using a novel shadowing growth technique"
https://doi.org/10.1088/0957-4484/20/46/465609

[42] M. J. O'Keefe and J. T. Grant, J. Appl. Phys. 79 (1996) 9134–9141 "Phase transformation of sputter deposited tungsten thin films with A15 structure"
http://dx.doi.org/10.1063/1.362584

[43] Y.G. Shen and Y.W Mai, Mater. Sci. Eng. A 284 (2000) 176–183 "Influences of oxygen on the formation and stability of A15 β-W thin films"
https://doi.org/10.1016/S0921-5093(00)00745-0

[44] S. M. Rossnagel, I. C. Noyan, C. Cabral Jr., J. Vac. Sci. Technol. B 20 (2002) 2047–2051 "The Phase Transformation of Thin Sputter-deposited Tungsten Films at Room Temperature"
http://dx.doi.org/10.1116/1.1506905

[45] Liang Chen, Toh-Ming Lu, Gwo-Ching Wang, Thin Solid Films 539 (2013) 65–69, "Creation of biaxial body center cubic tungsten nanorods under dynamic shadowing effect"
https://doi.org/10.1016/j.tsf.2013.04.151

[46] I. A. Weerasekera, S. Ismat Shah, David V. Baxter and K. M. Unruh, Appl. Phys. Lett. 64 (1994) 3231–3233 **"**Structure and stability of sputter deposited beta-tungsten thin films"
http://dx.doi.org/10.1063/1.111318

[47] Ananya Chattaraj, Mohammad Balal, Ashok Kumar Yadav, Sudipta Roy Barman, Anil Kumar Sinha, Shambhu Nath Jha, Sebastien Joulie, Virginie Serin, Alain C laverie, Vijay Kumar and Aloke Kanjilal, Sci. Rep. 10 (2020) 14718 (10pp) "Unravelling oxygen driven α to β phase transformation in tungsten"
https://doi.org/10.1038/s41598-020-71650-2

[48] Y. G. Shen and Y. W. Mai, J. Mater. Sci. 36 (2001) 93–98 "Structure and properties of stacking faulted A15 tungsten thin films"
https://doi.org/10.1023/A:1004847009613

[49] Katayun Barmak and Jiaxing Liu, J. Vac. Sci. Technol. A 35 (2017) 061516 (6pp) **"**Impact of deposition rate, underlayers, and substrates on β−tungsten formation in sputter deposited films" https://doi.org/10.1116/1.5003628

[50] Richard Tran, Zihan Xu, Balachandran Radhakrishnan, Donald Winston, Wenhao Sun, Kristin A. Persson and Shyue Ping Ong, Sci. Data 3 (2016) 160080 (13pp) "Surface energies of elemental crystals"
https://doi.org/10.1038/sdata.2016.80

[51] David R. Lide, CRC Handbook of Chemistry and Physics, 72nd Edition, CRC Press, Boca Raton, 1991

Table 1: Deposition rate and columnar tilt angle (β angle) for W thin films prepared at low (LP) and high (HP) pressures with different IW_2 target currents.

	0.33 Pa (LP)		1.5 Pa (HP)	
IW_2 target current (mA)	Deposition rate ($nm.min^{-1}$)	β angle (°)	Deposition rate ($nm.min^{-1}$)	β angle (°)
50	8.2	39	17.7	11
100	11	22	13.2	18
140	10.4	16	19.7	10
200	10.5	15	22.3	3
250	12.5	3	25.5	8

List of figures

Figure 1: Schematic representation of the OAD setup. Two tungsten targets W_1 and W_2 are tilted with fixed angles $\alpha W_1 = \alpha W_2 = 80°$. The target-to-substrate distances are fixed to 65 mm for W_1 and to 95 mm for W_2. The substrate can be fixed or rotated following the ϕ angle (not used in this study). W atoms are deposited on substrate defining a x-y plane whereas the z-axis is defined by the direction perpendicular to the substrate.

Figure 2: Top-view scanning electron microscopy observations of W thin films deposited at a) low pressure and b) high pressure with a constant target current (IW_1 = 140 mA) and various IW_2 target currents.

Figure 3: Cross-section scanning electron microscopy observations of W thin films deposited at a) low pressure and b) high pressure with a constant target current (IW_1 = 140 mA) and various IW_2 target currents.

Figure 4: X-ray diffraction patterns recorded in θ/θ configuration of W thin films prepared at low (LP) and high (HP) pressures with different IW_2 target currents: a) between 30° and 45°, b) zoom of the peak attributed to α-W (110) and β-W (210) superposition at around 40° (samples deposited at low pressure) and c) between 30° and 45° (increased y-scaling) for samples deposited at high pressure.

Figure 5: a, d) {200}, b, e) {210} and c, f) {211} x-ray reconstructed pole figures (RPF) for the W thin film deposited at low pressure with IW_2 = 200 mA. The direction of the incident fluxes, indicated by arrows corresponds to the rolling direction. The crosses correspond to theoretical texture of {100} <011> (a-c) and {211} <0-11> (d-f).

Figure 6: TEM images of columnar W thin films deposited at a) high pressure and b) low pressure with IW_2 = 200 mA. c) HRTEM image of a crystallized area acquired for the sample grown at low pressure and d) its fast Fourier transform (FFT) pattern corresponding to [001] zone axis of β-W.

Figure 7: DC electrical resistivity and resistivity anisotropy measured at room temperature as a function of the IW_2 target current for W thin films prepared by OAD with two W targets (IW_1 = 140 mA) at a) low (p = 0.33 Pa) pressure and b) high (p = 1.5 Pa) pressure.

- Nanocolumnar tungsten thin films are co-sputter deposited from two opposite sources.
- The column tilt angle is tunable at low sputtering pressure changing one current target.
- A cauliflower morphology is systematically produced at high sputtering pressure.
- Pressure and target current both influence electrical conductivity of nanocolumnar films.

Declaration of interests

☒ The authors declare that they have no known competing financial interests or personal relationships that could have appeared to influence the work reported in this paper.

☐The authors declare the following financial interests/personal relationships which may be considered as potential competing interests: